Modelling Winter Atmospheric River Frequency over the Western Himalayas Using Large-Scale Climate Modes Via Statistical Approach

Mohammad Humza Kanth[1], Sheikh Imran Fayaz[1], Munir Ahamd Nayak[1]

kanthhumza@gmail.com, sheikhimranfayaz@gmail.com,munir.nayak@nitsri.ac.in

This manuscript is a non-peer-reviewed preprint submitted to EarthArXiv.

Keywords

Atmospheric Rivers; Climate Modes; Himalayas; Generalized Linear Models; Generalized Additive Models

[1]Department of Civil Engineering, National Institute of Technology Srinagar, India

Abstract

Winter Atmospheric Rivers (ARs) contribute substantially to precipitation in the Western Himalayas, but how large-scale climate modes jointly influence their frequency remains unclear. In this study, we use a statistical method that combines correlation, phase-composite analysis of Integrated Vapor Transport (IVT), and predictive models such as linear regression, Generalized Linear Models (GLMs), and Generalized Additive Models (GAMs). We examine eighteen climate indices and data from 39 winters (1980 to 2018) and discover that the Arctic Oscillation, Pacific Decadal Oscillation, Pacific North American pattern, East Atlantic Western Russia pattern, and the Siberian High are strongly associated with winter AR frequency. The phase-composite IVT analysis reveals a consistent moisture-transport signal for each pattern. We also find that no one climate mode can account for the variability in ARs. However, including linear interaction terms in a GLM yields better predictions than a simple linear model. In contrast, a GAM that accounts for nonlinear relationships and key interactions, such as among the East Pacific–North Pacific, Western Pacific, and PNA patterns, provides considerably better predictive ability than a GLM. This indicates that AR frequency depends on nonlinear responses to the combined state of several climate modes. These results offer a statistical framework that clearly connects large-scale climate variability, including how different modes interact, to the frequency of winter ARs in the Western Himalayas. This connection helps improve seasonal forecasts and water resource planning in this challenging and data-limited region.

1. Introduction

Atmospheric rivers (ARs) are long and thin bands of concentrated water vapour in the lower atmosphere and are an important factor in local precipitation (Zhu & Newell, 1998; Payne et al., 2020)The occurrence of ARs is closely connected with climate modes, which are recurring, though not perfectly periodic, large-scale patterns of atmosphere–ocean variability that oscillate over months to years (McGregor, 2024; Guan & Waliser, 2015). Research has shown that the frequency and occurrence of ARs vary considerably according to the phase of the climate mode, thus affecting regional rainfall and the water cycle (Guan & Waliser, 2015 ;Nash et al., 2022; Yang et al., 2024). The effects of a climate mode are not confined to its area of origin; for instance, the El Niño–Southern Oscillation (ENSO) starts in the tropical Pacific but can affect the weather a long way away, a phenomenon known as teleconnection. Depending on its phase, a climate mode can either increase or decrease the likelihood of AR activity, and this impact can vary from one region to another. It is common for several climate modes to be active at the same time and for them to interact in order to determine AR patterns (McGregor, 2024;Wallace & Gutzler, 1981).

Research at global scale indicates that large-scale climate patterns can have a strong impact on the frequency and intensity of ARs, as well as on their routes and the amount of rainfall they bring. Nevertheless, the strength and direction of these effects differ according to region and season. Guan & Waliser (2015) found that ENSO, the Madden–Julian Oscillation (MJO), the Arctic Oscillation (AO), and the Pacific–North American pattern (PNA) all contribute significantly to the nature of winter AR activity on a global scale. For instance, El Niño generally leads to an increase in the frequency of ARs in a number of subtropical and extratropical regions, whereas the MJO, AO, and PNA affect AR occurrence linked to the large-scale circulation anomalies.

Studies at a regional level offer a more detailed examination of this subject. In western North America, Guan et al. (2012) discovered that the phase of the MJO has a strong effect on high-impact AR landfalls in the Sierra Nevada region. Mundhenk et al. (2018) demonstrated that combining the states of the MJO and the Quasi-Biennial Oscillation (QBO) can be used to predict landfalling ARs on a subseasonal basis. Other research carried out in the North Pacific and western North America has associated ENSO and Pacific decadal variability with year-by-year changes in AR activity (Gershunov et al., 2017; Xu et al., 2023). More recently, Yang et al. (2024) stated that the AO, QBO, ENSO, MJO, the Pacific Decadal Oscillation (PDO), and the PNA all influence AR clustering and orientation in the western United States, the main factors varying between early and late winter. With regard to the Atlantic side, Liet al. (2022) found that ENSO and the North Atlantic Oscillation (NAO) together determine when and where cold-season ARs take place.

Nash et al. (2022) discovered that large-scale climate patterns also have an effect on High Mountain Asia (HMA), since tropical storms over western and northwestern HMA occur more frequently during El Niño, positive AO, and negative Siberian High (Sib-H) conditions. This trend is not confined to HMA; for instance, in Northern California regional climate patterns such as the AO, PNA, Western Pacific Oscillation (WPO), and Eastern Pacific Oscillation (EPO) have a greater influence on precipitation from landfalling ARs than ENSO and can either enhance or reduce the effects of ENSO according to how they align (Guirguis et al., 2019). Generally, these studies indicate that variability in ARs is closely linked to the wider climate system, but the impact of each mode and the way they interact can differ considerably from region to region (Xu et al., 2023).

Not only do climate modes have an effect on the times at which ARs occur, but they also influence how well the ARs can be forecasted. DeFlorio et al. (2018) observed that the skill of subseasonal AR forecasts increased during El Niño in the North Pacific and in the western United States, as well as during negative AO conditions in the North Atlantic and in the United Kingdom. The greatest improvements in forecast skill occurred when the phases of ENSO and PNA were aligned. These 'forecasts of opportunity' indicate that large-scale climate information could make AR prediction frameworks more effective. Taken as a whole, the results show that climate modes provide valuable insights into AR variability and could enable climate information to move from being a diagnostic tool to being a means of predicting regional AR frequency.

Statistical methods have already demonstrated this potential in a number of fields. For example, Lavers et al. (2012) applied a Poisson regression model to examine the number of winter AR events in the British Isles by means of large-scale climate indices and found that count-based statistical models can be used for measuring the variability in AR frequency. Subsequent research has since extended climate-based forecasts to other areas and different time scales: Zhou & Kim (2018) investigated the prediction of winter AR frequency over the North Pacific in relation to ENSO, Castellano et al. (2023) developed a statistical subseasonal forecasting tool for AR activity in California based on MJO and QBO conditions, and Dong et al. (2024) demonstrated that monthly and seasonal predictions of AR frequency over the eastern United States were possible using the PNA. Altogether, these studies verify the predictive value of large-scale climate information and indicate that the main factors responsible for AR activity can vary considerably regionally.

It is clear from the evidence that climate modes have an impact on the occurrence of ARs in High Mountain Asia (Nash et al., 2022), but it is still not known how various large-scale climate modes together affect the frequency of ARs in the Western Himalayas. Findings from broader regions cannot be directly applied in this case since the influence of climate modes on AR activity differs from place to place. Moreover, although some other areas have observed nonlinear effects of climate modes on ARs (Xu et al., 2023), we still do not know how the frequency of ARs in the Himalayas responds to different climate modes, either in a linear or nonlinear way. Since climate modes can jointly influence AR activity, it is necessary to investigate their interactions, as the effect of one mode may depend on that of another (Guan et al., 2012; Mundhenk et al., 2018: Li et al., 2022; Xu et al., 2023). In order to address these uncertainties, this study develops a statistical framework to model and predict the number of winter ARs in the Western Himalayas by making use of several large-scale climate indices. A generalized linear model (GLM) is employed to examine approximately linear relationships between the climate indices and AR counts (McCullagh & Nelder, 2019). A generalized additive model (GAM) is also used, as it enables nonlinear responses, such as thresholds or non-monotonic patterns, to be present in the data (Hastie & Tibshirani, 2017; Wood, 2017). Both models include interaction terms between the climate modes, for example Sib-H × AO, East Pacific–North Pacific (EPNP) × PNA, PNA × Niño4, and Western Pacific (WP) × EPNP. Some of these are supported by established relationships in the literature like Sib-H × AO and PNA × Niño4 (Gong et al., 2001; W. Li & Forest, 2014), while the EP-NP × PNA and WP × EPNP terms are motivated by indirect evidence of shared North Pacific jet and circulation mechanisms linking these modes (Athanasiadis et al., 2010; Linkin & Nigam, 2008; Toride & Hakim, 2021). All interaction terms are retained only where they improve on the additive model. By comparing the linear and nonlinear effects and by looking at the interactions between these modes, we hope to determine which climate signals are most closely associated with variability in ARs in the Western Himalayas and how well they predict the frequency of winter ARs. To our knowledge, this is the first study to apply and compare both GLM and GAM to the frequency of winter ARs in the Western Himalayas, using several large-scale climate indices and directly testing their linear, nonlinear, and interactive effects.

2. Data

The study focuses on winter ARs in the western Himalayan area, covering latitudes from 29°N to 37°N and longitudes from 72°E to 81°E. It makes use of meteorological data from ERA5, which is the fifth-generation atmospheric reanalysis produced by the European Centre for

Medium-Range Weather Forecasts (ECMWF). ERA5 has a horizontal resolution of 0.25° × 0.25° (approximately 31 km worldwide), includes 37 vertical pressure levels, and provides data on an hourly basis. For this research, data were gathered at six-hour intervals (00, 06, 12 and 18 UTC) during the winter period (from December to February) between the years 1980 and 2018. The integrated vapor transport (IVT; in kg m^{-1} s^{-1}) was computed from the ERA5 data by employing 20 pressure levels ranging from 1000 to 300 hPa (McCarty et al., 2016; Gelaro et al., 2017), in accordance with the formula given below:

$$IVT = \sqrt{\left(\frac{\int_{1000}^{300} qudp}{g}\right)^2 + \left(\frac{\int_{1000}^{300} qvdp}{g}\right)^2}$$

In this context, q denotes specific humidity (in kg kg^{-1}), u and v represent the zonal and meridional wind components (in m s^{-1}), p is the pressure level (in hPa), and g stands for gravitational acceleration (in m s^{-2}). Table S2 gives the number of winter atmospheric rivers over the Western Himalayas for each year from 1980 to 2018 (Nayak et al., 2021). Each winter (DJF) is named according to the year in which January and February take place; for instance, 'winter 1981' includes the period from December 1980 to February 1981.

The study looks at 18 climate modes in order to evaluate their possible influence on the frequency of winter AR occurrences in the Western Himalayas. The monthly index values for Niño3, Niño4, the Southern Oscillation Index (SOI), the Dipole Mode Index (DMI), the PDO, and the Atlantic Multidecadal Oscillation (AMO) were obtained from the NOAA Physical Sciences Laboratory climate indices archive. The monthly values for NAO, AO, WP, EPNP, PNA, the East Atlantic pattern (EA), the East Atlantic–Western Russia pattern (EA-WR), the Antarctic Oscillation (AAO), and the Scandinavian pattern (SCP) were sourced from the NOAA Climate Prediction Center teleconnection indices. The Tropical Western–Eastern Indian Ocean (TWEIO) index, the Equatorial Indian Ocean Oscillation (EQ) and the Siberian High (Sib-H) index were calculated using the approaches outlined by Abid et al. (2020),Gadgil et al. (2004), and Panagiotopoulos et al. (2005), respectively.

In each case, we calculated the average of the monthly index values for December, January, and February (DJF) in order to arrive at one DJF value. We then correlated these seasonal climate-index values with the frequency of AR occurrences in the winter. For instance, if winter 1980 includes the period from December 1979 to February 1980, match the AR count for winter 1980 with the average climate-index value computed from December 1979, January 1980, and February 1980.

3. Methods

The study uses a multi-stage statistical method to identify the climate patterns that affect winter AR activity in the Western Himalayas and to develop a predictive model for AR frequency.

In the first stage, the Pearson correlation coefficient is used to examine the strength and direction of the relationship between each climate mode index and the number of winter ARs. This correlation analysis screens the climate modes and identifies those with a statistically meaningful relationship with winter AR frequency. The selected climate modes are then used to analyze AR frequency modulation.

In the second stage, we look at each climate mode during both its positive and negative phases. For each mode, Welch's two-sample t-test for unequal variances compares the mean IVT in the positive phase with the mean IVT in the negative phase and examines whether there is a significant difference in the mean IVT between the two phases, thus allowing us to determine which phases of the climate mode are associated with an enhanced or suppressed moisture transport over the area.

In the end, the climate modes that proved statistically significant in the first two stages are used as predictors, in combination with the modes affecting their occurrence, within both the GLM and GAM approaches. Because Poisson regression is suitable for a count response variable (the number of winter ARs), both models use it. They are then compared to determine which best describes the relationship between the frequency of winter ARs and the climatic indices, including their interaction effects.

3.1 Analysis using the Pearson Correlation

In order to find out which climate modes are most relevant to winter AR activity in the Western Himalayas, we determined the Pearson correlations between each climate mode index and the winter frequency of ARs. For each winter (DJF) season, we calculated the mean value of each climate mode index and compared it with the events that occurred during that winter, using the AR frequency dataset for the Himalayan region for 1980–2018 (Table S2).

We applied this procedure to each climate mode index examined in the study. For each climate mode, we calculated the p-value by turning the correlation coefficient into a test statistic and comparing it with the appropriate reference distribution. Given the sample size in the present study ($n = 39$ winters), we assessed the significance of each correlation coefficient using a t-distribution with $n - 2$ degrees of freedom, in accordance with the standard method for testing the significance of a Pearson correlation coefficient.

To obtain the p-value, we compared the test statistic to the t-distribution. The p-value is the probability of observing a correlation as extreme or more extreme than the one observed, assuming the null hypothesis that no true linear relationship exists between the climate mode and the frequency of winter AR events. We regarded climate modes with p-values less than 0.13 as potentially relevant predictors and included them in the phase-wise analysis described in Section 3.2.

3.2 A composite analysis of the phases of the climate mode (using Welch's t-test)

Although the Pearson correlation (Section 3.1) can show whether a climate mode is statistically linked to the frequency of winter AR events, the correlation coefficient alone does not prove this association reflects a genuine and physically meaningful change in the atmosphere's moisture-transport environment. It may instead reflect a few exceptional years rather than a consistent physical mechanism. To investigate this, a phase-wise and grid cell-wise composite analysis of the IVT was carried out for each significant climate mode identified in Section 3.1. This checked whether the positive and negative phases correspond to a clear and spatially coherent difference in the amount of moisture transported into the study area, since this is the physical variable through which a climate mode could plausibly affect AR frequency.

The climatic indices are adjusted to have a mean of zero and a standard deviation of one. Winters were considered in the positive phase if the index was above +0.5 standard deviations and in the negative phase if below −0.5 standard deviations. At each grid cell across the study area, we calculated the mean DJF IVT separately for positive- and negative-phase winters. This enabled us to determine differences in the strength and spatial coverage of AR-favorable moisture transport conditions between the two phases.

In order to find out whether there was a statistically significant difference in the mean IVT between the two phases, we carried out a two-sample t-test (more precisely Welch's t-test for unequal variances) at each grid cell, comparing the IVT distributions for the positive and negative phases at the 5% level of significance.

3.3 Using GLM and GAM to Predict AR Frequency

Before building the multivariate models, we first ran a simple linear regression of winter AR frequency on each significant climate mode. This showed how well each mode predicted AR frequency on its own and provided a baseline for comparison. Even though AR counts are discrete and not normally distributed, this step gave us a clear first estimate of how much AR frequency changes with each climate index. Neither the correlation analysis (Section 3.1) nor the phase composites (Section 3.2) provide this information. We used a t-test to check whether each regression coefficient differed significantly from zero, indicating a linear relationship between the climate mode and AR frequency. We also measured predictive performance using Leave-One-Out Cross-Validation (LOOCV) with RMSE to compare these results with the GLM and GAM models discussed later.

Although single-predictor linear regression is a useful baseline, it has two main drawbacks for our study. First, it assumes the response is continuous and normally distributed, but AR frequency is actually count data. Second, it examines each climate mode separately and cannot show how multiple modes might work together. GLMs and GAMs solve both problems by letting us model count data with the right distribution and include multiple modes and their interactions in one model.

GLM

The general form of a GLM is given by:

$$g(\mu_i) = \beta_0 + \beta_1 x_{i1} + \beta_2 x_{i2} + \cdots + \beta_n x_{in}$$

where $u_i = E(y_i)$ is the expected value of the response variable, $g(.)$ is the link function, $x_{i1,} \cdots, x_{in}$ are the predictor variables for observation i, and $\beta_o, \cdots, \beta_n$ are the coefficients estimated via Maximum Likelihood Estimation.

In this study, since the response variable (number of winter ARs) represents count data, a Poisson distribution with a log link function was used, giving:

$$\log\big(E(ARs)\big) = \beta_0 + \beta_1 x_1 + \beta_2 x_2 + \cdots + \beta_n x_n$$

In this case, each x stands for a climate mode that has been found to be statistically significant (or an interaction between two modes, for example Sib-H × AO), as described in Sections 3.1 and 3.2. The model was fitted by taking into account all of the significant modes and their relevant interactions at the same time, which enabled the combined and joint effects of several climate drivers on the frequency of AR events to be measured in a single equation, a point that the single-predictor regression in (Text S1) was unable to address.

GAM

The general form of a GAM extends the GLM by replacing the linear predictor terms with smooth, non-parametric functions:

$$g(\mu_i) = \beta_0 + f_1(x_{i1}) + f_2(x_{i2}) + \cdots + f_n(x_{in})$$

where each f_i is a smooth function of a predictor, estimated from the data using basis splines rather than assumed to follow a fixed linear form:

$$f_i(x_i) = \sum_{k=1}^{K_j} \beta_{jk} b_{jk}(x_j)$$

Again using a Poisson distribution with a log link (consistent with the GLM), this becomes:

$$\log\big(E(ARs)\big) = \beta_0 + f_1(x_1) + f_2(x_2) + \cdots + f_n(x_n)$$

In this study, GAM was employed in this study to determine whether the relationships between climate modes and the frequency of winter AR events are nonlinear, since the GLM is unable to do so as it assumes that the effect of each predictor must be a straight line in log-space. The smooth terms were fitted using a certain number of basis splines (n) and a smoothing parameter (λ), and it is these two elements that decide how flexible or smooth the resulting curve is; a smaller λ results in greater wiggliness and thus in a better capture of sharp nonlinear patterns, whereas a larger λ leads to a smoother and more linear-like fit.

How the two models were used together

GLM and GAM were evaluated on the basis of four criteria: the RMSE, the log-likelihood, the Akaike information criterion (AIC), and the pseudo R^2. The RMSE measures the average prediction error and shows how closely the model's predicted numbers of AR match the observed values. The log-likelihood shows the probability of the observed data given the fitted model, higher (less negative) values meaning that the fit is better. The AIC includes the log-likelihood and imposes a penalty for extra parameters, so that lower AIC values indicate a more optimal balance between fit and complexity. Pseudo R^2 measures the improvement in model fit compared with a null model that contains only an intercept, this being similar to the ordinary R^2 in linear regression.

We applied both the GLM and the GAM using the same set of significant climate modes and their interactions so that a direct comparison could be made. The GLM examined whether a linear combination of the predictors (in log-space) was able to account for AR frequency. The GAM investigated whether nonlinear and flexible relationships would lead to an improvement in the results. The models were assessed using LOOCV across 39 winters and were compared with one another and with the linear regression baseline using RMSE, Log-Likelihood, AIC, and Pseudo R-squared.

4. Results

This section shares the results of the multi-stage statistical analysis described in Section 3. The goal is to find the climate modes that influence winter AR variability over the Western Himalayas and to develop a model to predict AR frequency. The results are presented in the same order as the methods.

4.1. Identification of Significant Climate Modes

We performed a Pearson correlation (r) analysis between each of the eighteen climate mode indices and the winter frequency of ARs over the Western Himalayas from 1980 to 2018. This helped identify which modes had a significant monotonic relationship with AR activity. The r and p-values are shown in Table 1. Using a relaxed significance level of α=0.13, which fits the small sample size (n=39 winters) and the exploratory purpose of this step, AO, PDO, PNA, EA-WR, and Sib-H showed significant correlations with winter AR activity. This suggests they could be useful predictors in the modeling framework. The other climate modes had weak or non-significant correlations (p>0.13) and were not included in further analysis.

Table 1. Pearson correlation (r) between annual winter AR frequency and climate mode indices over the Western Himalayas, with corresponding statistical significance (p-values), 1980–2018.

Mode	r	*p*-value	Mode	r	*p*-value	Mode	r	*p*-value
Niño3	0.006	0.970	**AO**	**0.273**	**0.093**	AAO	−0.056	0.737
Niño4	0.012	0.944	WP	0.118	0.474	SCP	−0.154	0.349
SOI	−0.024	0.884	EPNP	−0.009	0.957	TWEIO	0.118	0.475
PDO	**−0.318**	**0.049**	DMI	0.130	0.430	EQ	0.109	0.510
AMO	−0.053	0.749	EA	−0.052	0.753	**Sib-H**	**−0.249**	**0.127**
NAO	−0.092	0.578	**PNA**	**−0.311**	**0.054**	**EA-WR**	**0.337**	**0.036**

4.2. Climate Mode Phase Attribution

In order to investigate the relationship between different climate modes and the frequency of winter AR occurrences, we compared the DJF-mean IVT for the positive and negative phases of the AO, PDO, PNA, and EA-WR patterns from 1980 to 2018. Since Nash et al. (2022) had previously shown the link between Sib-H and AR-favorable moisture transport over High Mountain Asia, we decided not to include Sib-H. They found that ARs happen more frequently when the Sib-H phase is negative, which is in agreement with the negative correlation that we have observed (Table 1). By using the phase-composite method, we examined whether the statistical association between each of the remaining modes and AR frequency also exhibited a consistent difference in moisture transport between its two phases. A Welch's two-sample t-test was carried out at the 5% significance level, and only those grid cells that showed statistically significant phase differences ($p < 0.05$) were included in the composite difference maps.

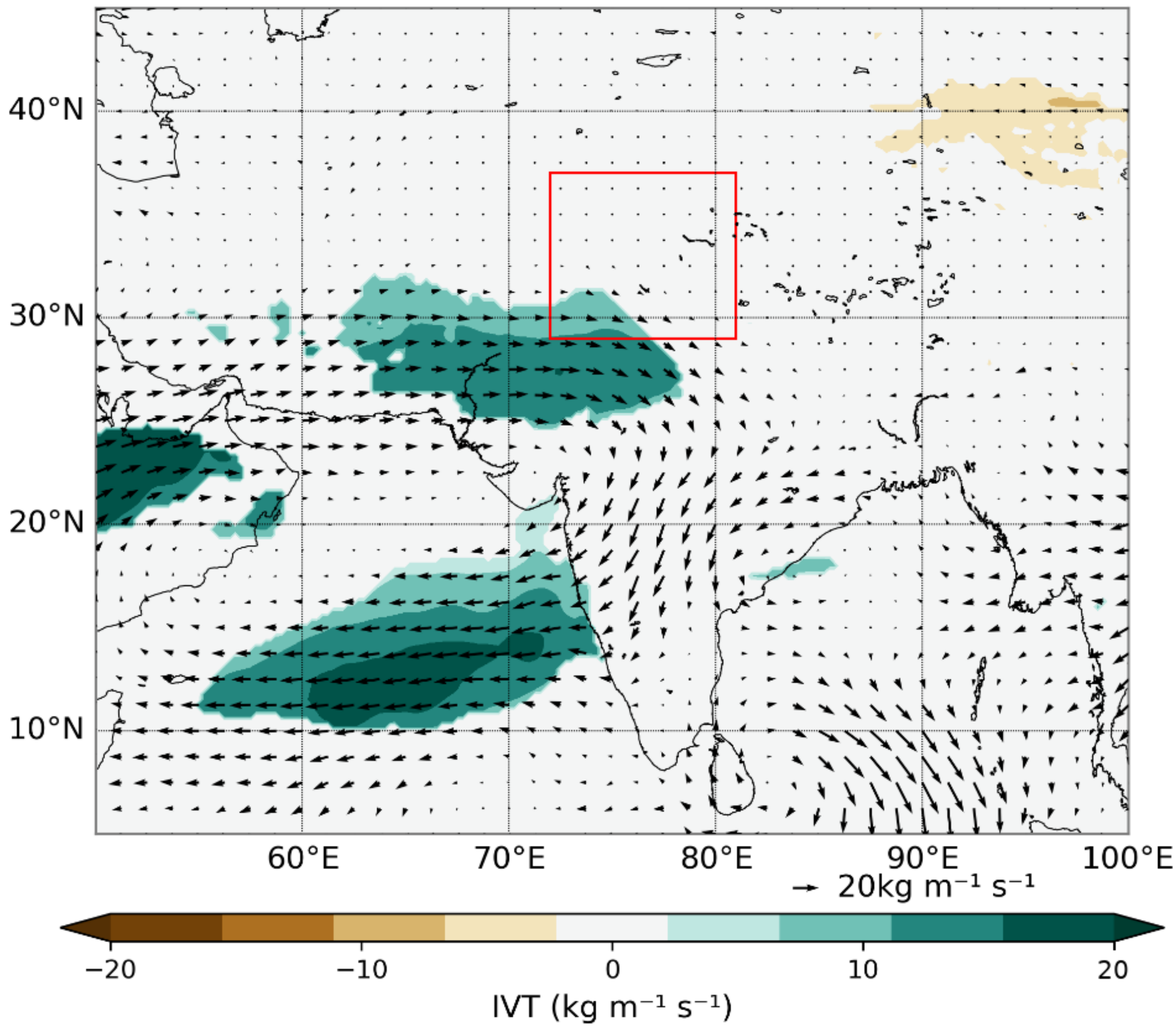

Figure 1. Composite differences in IVT between AO+ and AO− phases over the Western Himalayas from 1980 to 2018. Only differences statistically significant at or above the 95% confidence level (Welch's two-sample t-test, $p<0.05$) are shaded.

Figure 1 shows the combined difference in the DJF mean IVT between the AO+ and AO− phases, but only for grid cells where this difference is found to be statistically significant according to Welch's t-test at the 5% level. In the AO+ phase, significantly higher IVT appears as a zonally extended band near 27–30°N, stretching across the area just south of the study region and extending all the way to its southern boundary (indicated by the red box). Nash et al. (2022) recorded a similar increase in IVT during AO+ minus AO− over southwest Asia, this being linked to an anticyclonic anomaly over the Arabian Sea, in the case of ARs affecting High Mountain Asia. Although the significant signal does not reach within the entire study box, its position just upstream of it implies that there is an enhanced moisture-transport pathway during AO+. Such conditions are conducive to ARs occurring over the Western Himalayas.

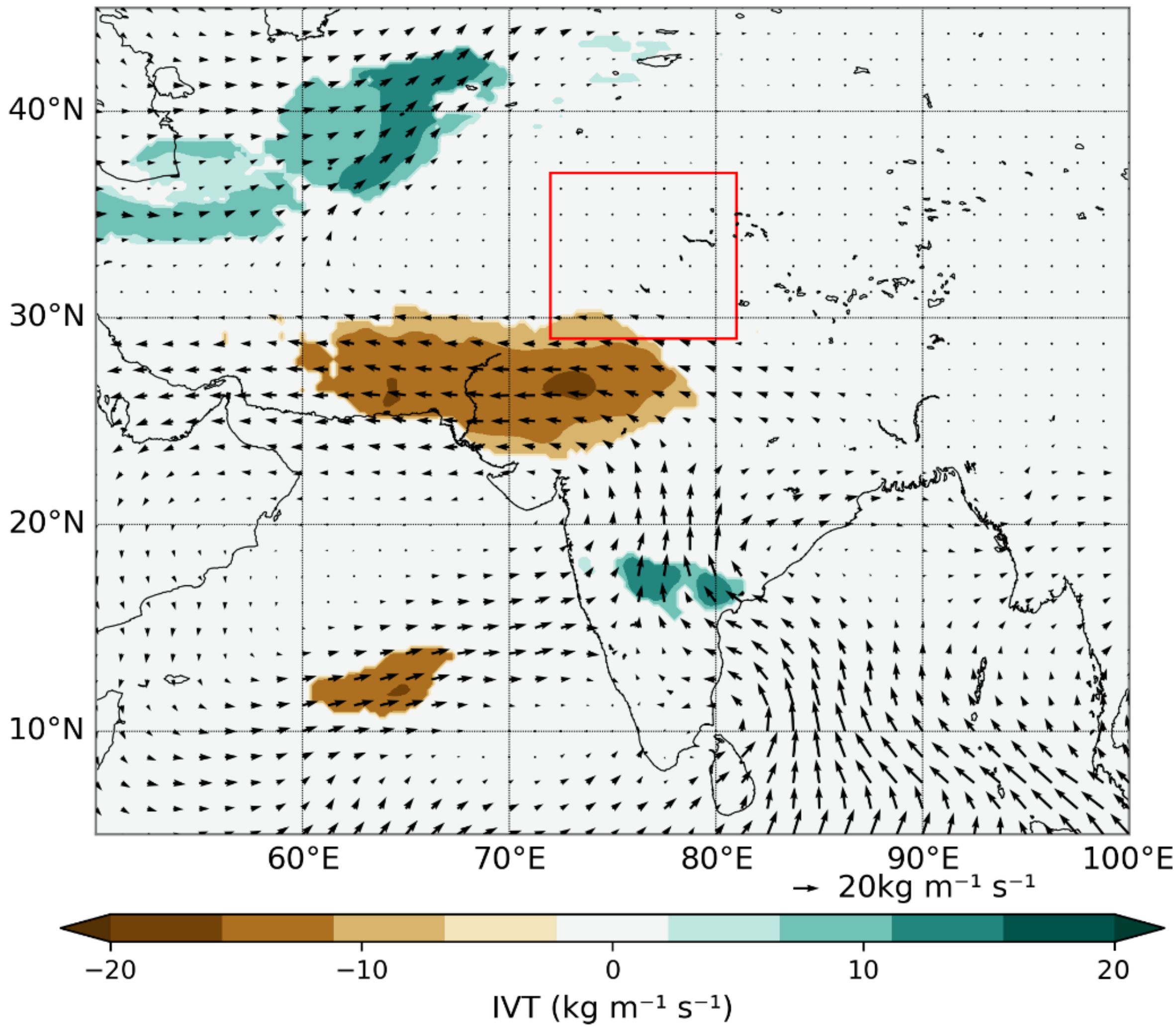

Figure 2. Composite difference in IVT between PDO+ and PDO− phases over the Western Himalayas.

As with AO, DJF-mean IVT was compared between the positive and negative phases of the PDO. Figure 2 shows the composite difference (PDO+ minus PDO−) at grid cells passing Welch's t-test at the 5% significance level. The dominant significant signal is a zonally elongated band of negative difference along roughly 25–30°N, located to the south and southwest of the study domain (red box), indicating higher IVT during the negative phase of the PDO. Positioned immediately upstream of the domain, this band of enhanced moisture transport represents conditions favourable to AR development and propagation toward the Western Himalayas during PDO−. This is consistent with the negative correlation between the PDO and winter AR frequency found at the screening stage (Table 1, $r=-0.318$), supporting the retention of PDO as one of the stronger predictors carried into the modelling stage.

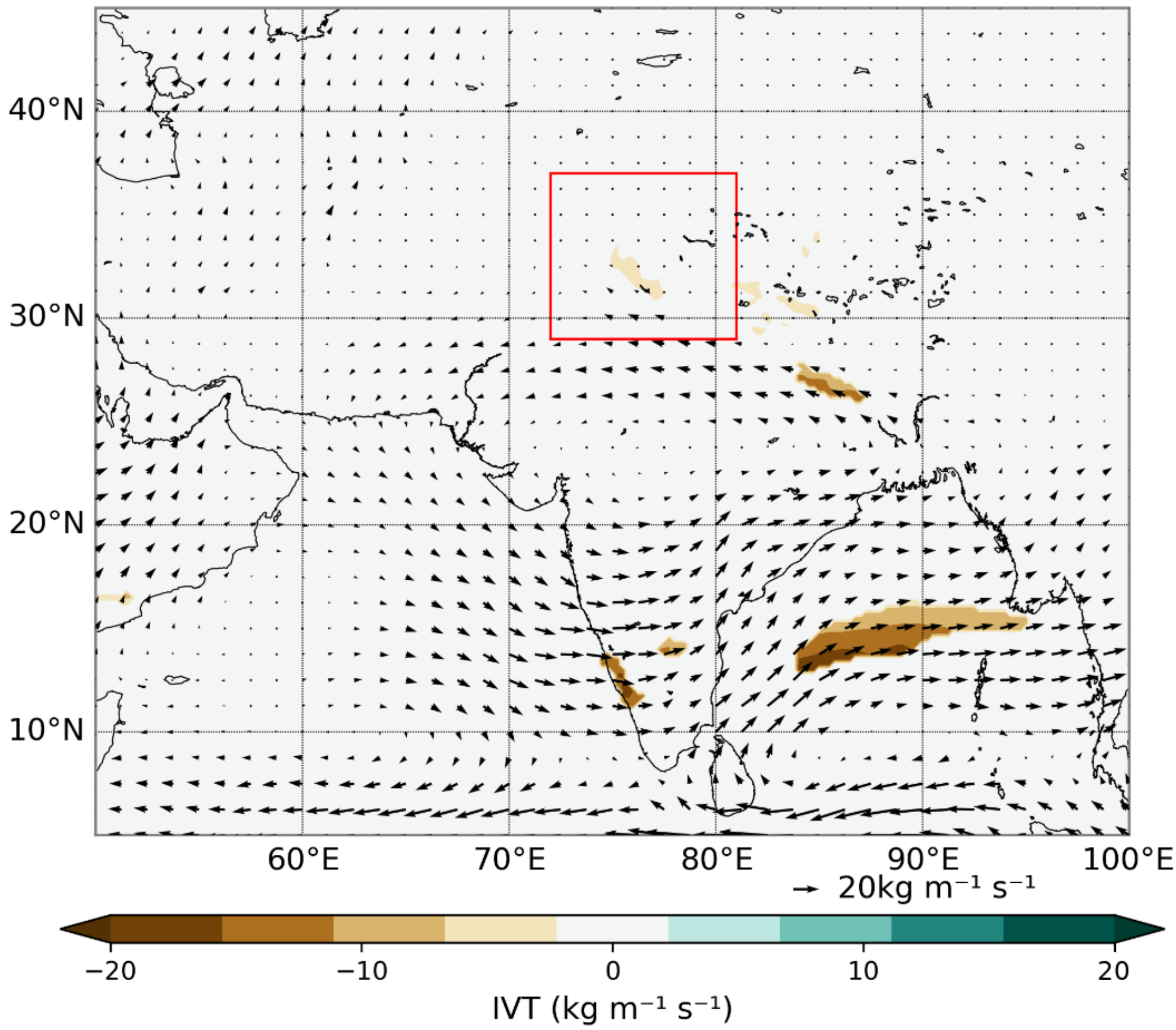

Figure 3. Composite difference in IVT between PNA+ and PNA− phases over the Western Himalayas.

In comparison with AO and PDO, the PNA displays a weaker and more diffuse signal in Figure 3, with only a small region showing a significant IVT difference in the Western Himalayas. In the cases where there is a significant difference, it is negative, indicating that IVT is greater during the negative phase (PNA−). This is in agreement with the negative correlation between PNA and winter AR frequency that was previously found (Table 1, $r = -0.311$) and is similar to the direction observed for PDO, which is positively associated with PNA (Chen et al., 2023). Although the PNA does not produce a clear and large-scale moisture transport pattern like AO and PDO, its consistent relationship with AR frequency and its presence in the interaction terms of the multivariate models show that it still contains useful information regarding winter AR variability in the Western Himalayas.

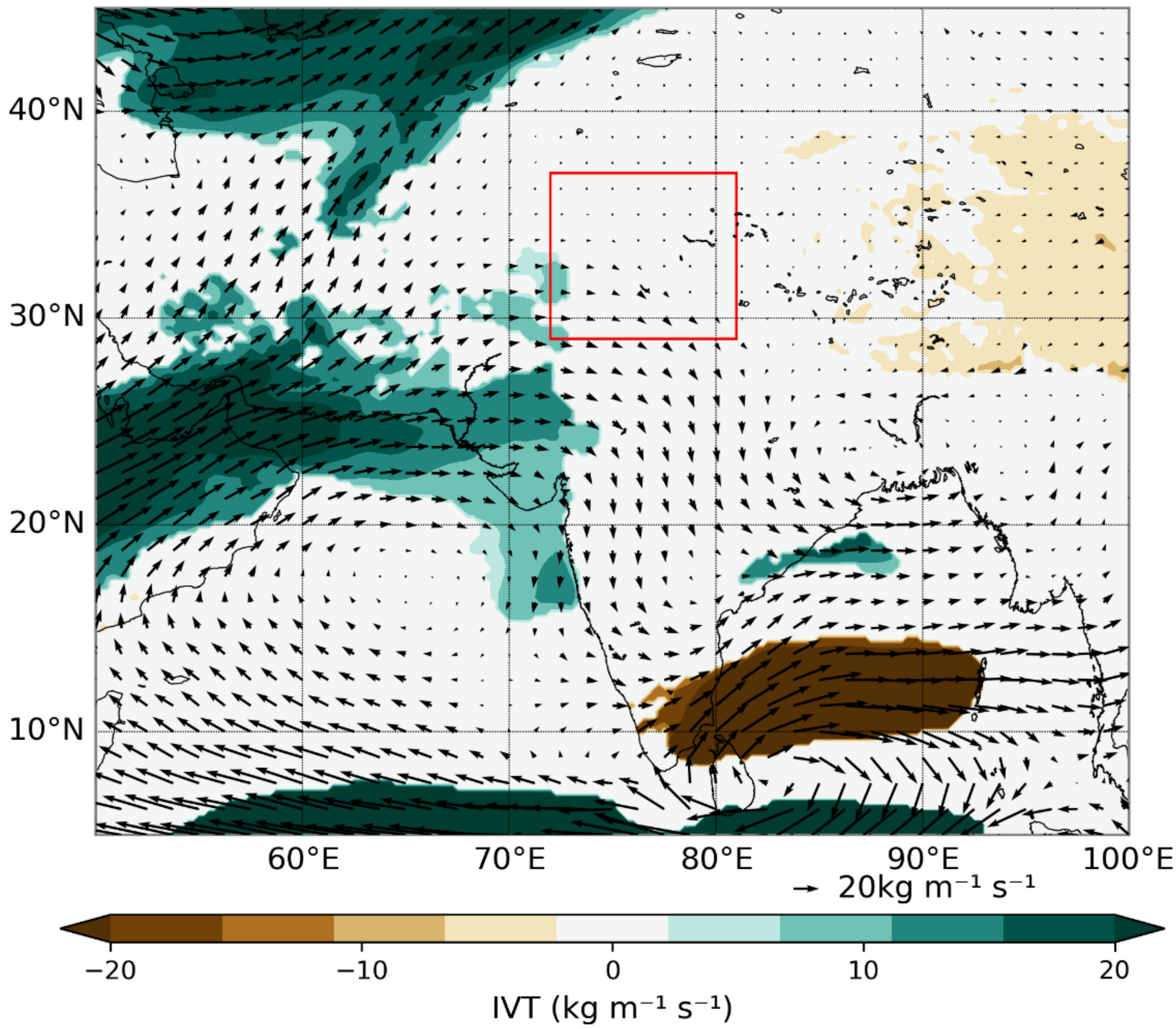

Figure 4. Composite difference in IVT between EA-WR+ and EA-WR− phases over the Western Himalayas.

A similar analysis was carried out for the EA-WR pattern (Figure 4). Significant positive differences dominate the western part of the domain, indicating higher IVT during the positive phase (EA-WR+), with the signal extending into the western edge of the study box (red box). This band of enhanced moisture transport, situated across and immediately upstream of the domain, represents conditions favourable to AR occurrence over the Western Himalayas during EA-WR+. This is consistent with the positive correlation between EA-WR and winter AR frequency found at the screening stage (Table 1, r=0.337 and p=0.036), the strongest positive correlation among the modes tested.

Taken together, the phase-composite analysis shows that the sign of the IVT response matches the correlation found at the screening stage for every mode examined: AO+ and EA-WR+ are associated with enhanced moisture transport, while PDO− and PNA− show higher IVT over the Western Himalayas. This agreement between two independent lines of evidence, one based on discrete AR counts and the other on a continuous atmospheric IVT field, indicates that these modes are not only statistically related to AR frequency but also correspond to real differences in the moisture-transport environment in which ARs develop. The analysis therefore provides physical support for retaining these modes as predictors in the statistical modelling of winter AR frequency that follows.

4.3. Multivariate Model Performance (GLM and GAM)

In supplementary Text S1 we examined how well individual climate modes predict winter AR frequency using single-predictor linear models. EA-WR emerged as the strongest standalone predictor (LOOCV RMSE 2.27, p=0.036), but RMSE values clustered narrowly between 2.27 and 2.33 across all five modes, and in every case the cross-validated predictions spanned a much narrower range than the observed AR counts. This indicates that no single climate mode captures a substantial share of the year-to-year variability in AR frequency. Here we build on that baseline by developing multivariate GLM and GAM frameworks that incorporate several climate modes together with their interactions, and we use the single-predictor RMSE range as a reference against which the multivariate models are compared.

GLM

The GLM was constructed using the climate modes which were found to be statistically significant in Section 4.1, together with various interaction terms involving those and other climate indices. It has been shown that AR activity is influenced by the combined state of several climate modes, not merely one (Nash et al., 2022; Guirguis et al., 2019; Soulard et al., 2019). We experimented with different combinations of predictors and interaction terms and selected the final model on the basis of the lowest AIC in order to achieve a balance between fit and complexity. The model retained EA-WR as a direct predictor and included the interaction terms Sib-H × AO, EPNP × PNA, and PNA × Niño4, resulting in the following equation:

$$\log\big(E(ARs)\big) = \beta_0 + \beta_1(Sib - H \times AO) + \beta_2(EA - WR) + \beta_3(EPNP \times PNA) \\ + \beta_4(PNA \times Nino4)$$

GAM

We used a Poisson distribution with a log link function to model the number of winter ARs in statistically significant climate modes and their interactions. Along with significant climate modes and their interactions, we included the EPNP × PNA and WP × EPNP interaction terms to find the lowest AIC for the GAM, on physical grounds, because these modes act on shared components of the North Pacific circulation. This provides a physical basis for modeling the effect of EPNP on winter AR frequency through its interaction with both WP and PNA, rather than treating EPNP as an independent linear predictor. The fitted model is given by:

$$\log\big(E(\text{ARs})\big) = \beta_0 + f_1(\text{EA-WR})\ (n = 6, \lambda = 0) + f_2(\text{EPNP} \times \text{PNA})\ (n = [6,6], \lambda = 2) \\ + f_3(\text{WP} \times \text{EPNP})\ (n = [5,5], \lambda = 0)$$

The number of basis splines employed in the construction of each smooth term is denoted by n and λ represents the smoothing (regularization) parameter.

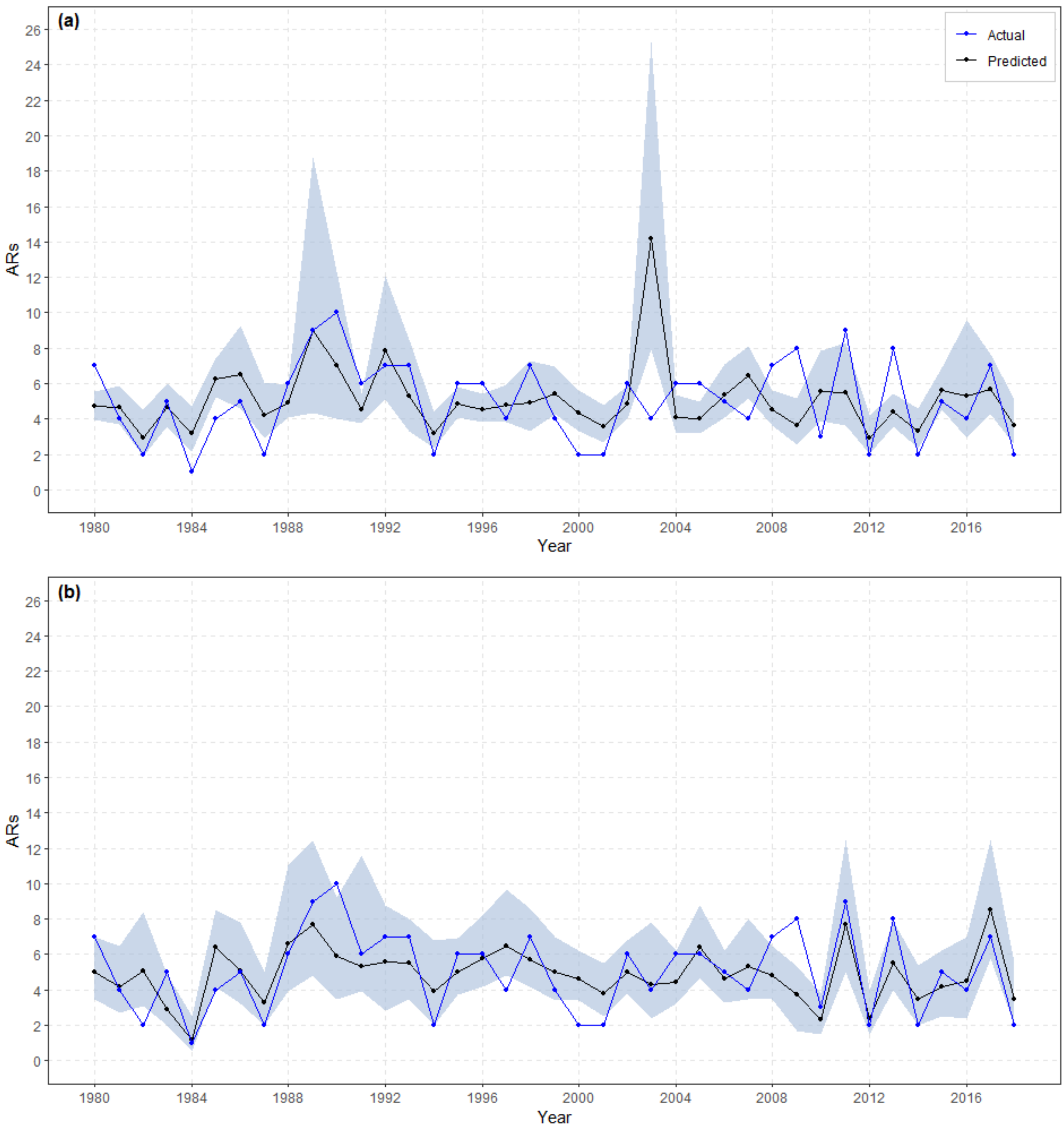

Figure 5. LOOCV results for (a) the GLM and (b) the GAM, showing observed (blue) and out-of-sample predicted (black) winter AR counts over 1980–2018. Shaded bands indicate 95% prediction intervals.

Figure 5 shows how the LOOCV predictions from both models compare to the observed data on the same vertical axis. The GLM (a) captures the general low-frequency changes in the observed series, but its predictions are much less variable. Except for two spikes, the model's predictions stay between about 3 and 7, while the actual counts range from 1 to 10. The biggest error happens in 2003, when the model predicts about 14 ARs, but only 4 were observed. This is the largest difference on record and the only time the prediction exceeds the observed maximum. The uncertainty band also widens substantially here, reaching nearly 25 ARs, suggesting that the climate conditions that year were not well represented in the data and that the model's interaction terms are unreliable. Since the dataset covers 39 years, this one year has a big impact on the RMSE. Still, this error is useful because it shows that the model's interaction terms become unstable when predictor combinations fall outside the range seen in the data.

The single-predictor linear models have LOOCV RMSE values between 2.27 and 2.33 (Table S1), slightly lower than the GLM's 2.50. However, interpret this difference carefully. Figure S2 shows that the linear models' predictions change very little from year to year, staying between about 4 and 6.5, while the actual counts range from 1 to 10. This low RMSE mostly comes from the models predicting close to the average each year, not from real predictive skill. For example, always predicting the mean gives an RMSE of 2.35, so the best single-predictor model is only about 3% better than a no-skill forecast. In contrast, the GLM captures much more of the year-to-year changes. Its higher RMSE is mostly due to a few unstable predictions, such as in 2003. If you leave out that year, the GLM's RMSE drops to about 2.04.

The GAM (b) is more stable. Its predictions stay within the observed range and reflect year-to-year changes that the GLM misses. For example, in 1984, the GAM predicts a minimum of 1.2, which is close to the observed value of 1, while the GLM predicts 3.2. In 2011, the GAM predicts 7.7 and the observed value is 9; the GLM predicts 5.5. For 2013, the GAM gives 5.5 compared to the observed 8, while the GLM predicts 4.4. In 2003, the GAM predicts 4.3, which is close to the observed 4, while the GLM predicts 14.2. While the GAM does not capture every detail and underestimates the 1990 maximum more than the GLM, its errors are moderate and spread throughout the record instead of being concentrated in a single unstable prediction.

Table 2 shows how both models performed. The GAM had a higher Log-Likelihood (−70.97 compared to −79.50) and a lower AIC (162.44 compared to 168.97), even though it used fewer estimated parameters. Its LOOCV RMSE was 1.74, which is much lower than the GLM (2.50) and the best single-predictor linear regression (2.27, Table S1). This means the GAM had the best out-of-sample predictive accuracy of all the models tested. The Pearson correlation between observed and predicted counts for the GAM was 0.65, about twice as high as the GLM's 0.31.

The GAM's pseudo $R^2$of 0.75 indicates that it accounts for a substantially larger share of the deviance relative to an intercept-only model than the GLM (0.34), implying that allowing nonlinear, flexible relationships captures more of the variability in winter AR occurrence than linear or additive effects alone. This relatively high value should nonetheless be treated with caution, since a flexible spline-based model fitted to only 39 winters carries a real risk of overfitting to the training sample even when performance is assessed by LOOCV.

Table 2. Model performance metrics for the GLM and GAM.

Model parameters	**GAM**	**GLM**
Log-Likelihood	-70.97	−79.50
AIC	162.44	168.97
RMSE	1.74	2.50
Pearson correlation	.65	0.31
Pseudo R^2	0.7547	0.34

No of variables	4	6

When the figure is combined with the statistical measures, the same conclusion is reached. The GLM appears to be stable because it predicts values close to the climatological mean, but it performs very poorly when making predictions beyond the range of well-sampled predictor combinations. Although its prediction intervals are narrow over most of the record, they include the observed value in only 38% of years, a great deal below the nominal 95% level. The GAM's nonlinear smooths follow the true interannual variability, and its broader intervals include the observed value in 74% of years. While neither model is fully calibrated at this sample size, the GAM performs better than the other models on all the evaluation criteria and provides a much more honest account of predictive uncertainty. This therefore supports the GAM as the preferred model for winter AR frequency over the Western Himalayas and shows that the relationship between large-scale climate variability and AR frequency in this area is substantively nonlinear.

5. Discussion

The application of Poisson regression to link the frequency of winter AR events with climate indices agrees with previous studies in other midlatitude areas. Lavers et al. (2012) used an AIC-based stepwise selection procedure, similar to the one employed in this study, to associate winter AR occurrences over Britain with climate variability and found that one predictor the SCP was enough to account for the interannual variation in ARs, there being more ARs when the SCP was in its negative phase. On the other hand, no single mode was dominant in controlling AR variability over the Western Himalayas; several modes (PDO, PNA, AO, EA-WR) exhibited similar predictive power, and in order to make a meaningful improvement in predictive ability interaction terms (Sib-H × AO, EPNP × PNA, WP × EPNP, PNA × Nino4), indicating a more complex multi-mode circulation control than that seen over the North Atlantic.

The climate modes identified here are broadly consistent with those reported for the wider High Mountain Asia region. Nash et al. (2022) found ARs reaching western and northwestern HMA to be significantly more frequent during positive AO and negative Siberian High conditions, matching the directions obtained in this study from the correlation and phase-composite analyses. The present study extends that set of modes, with PDO, PNA and EA-WR also emerging as relevant predictors over the Western Himalayas specifically, none of which was examined by Nash et al. One difference concerns ENSO, which they found to be significant across HMA but which showed no significant relationship with winter AR frequency here. Several differences in scope could account for this: their domain is considerably larger than the Western Himalayan box used here, their analysis spans DJFMAM rather than DJF alone.

Nash et al. (2022) noted that it is difficult to separate the effects of individual modes because they rarely act alone, and they suggested that future research should look at their combined influence. Our models address this by including interaction terms. For example, ENSO is not used as a direct predictor but is included through the PNA × Niño4 term, even though Niño4 by itself has only a weak correlation with AR frequency ($r = 0.012$). This matches other findings that ENSO affects Northern Hemisphere circulation mainly by influencing extratropical patterns like the PNA (Soulard et al., 2019; Li & Forest, 2014). Both the GLM and the GAM include interaction terms, but their impact is most clear in the GAM, which also uses nonlinear responses and performs better than both the linear baseline and the GLM on all evaluation measures. This suggests that winter AR variability in this region is shaped by the combined and partly nonlinear effects of several modes, rather than by any single mode alone.

Since the dataset includes only 39 winters, there is limited statistical power to screen climate modes. To keep physically reasonable predictors, a more relaxed significance threshold ($\alpha = 0.13$) was used. Both the GLM and GAM were fitted with relatively few observations compared to the number of parameters and interaction terms, so overfitting remains a concern, even though leave-one-out cross-validation was applied. The high pseudo R-squared for the GAM should be considered in this context. The interaction terms in the models were not analyzed on their own; their contribution was shown statistically through AIC-based selection and predictive skill, but they were not tested with the correlation or phase-composite analysis used for individual modes in Sections 4.1 and 4.2. As a result, their direct relationship with AR frequency and the moisture-transport field is not fully described. Finally, the results are based on a single reanalysis dataset, which could influence the findings, as shown in other multi-reanalysis studies (Lavers et al., 2012).

A natural extension of this work would be to apply the phase-composite approach used in Section 4.2 to the interaction terms themselves, compositing IVT on the joint phase states of interacting mode pairs, for example AO+ with Sib-H− against AO− with Sib-H+. The composites presented here characterise each mode individually and therefore cannot show how the moisture-transport field responds when two modes are in reinforcing or opposing states. Such an analysis would also allow the interaction effects to be interpreted against the mechanisms already described in the literature. Establishing whether the improvement in predictive skill from these terms corresponds to identifiable changes in the spatial structure of moisture transport, and whether those changes are consistent with the circulation mechanisms reported in the studies, would provide a physical basis for interaction effects that the statistical models currently capture only implicitly.

The analysis presented here covers 1980–2018, but ERA5 extends to the present, so the record can be lengthened immediately by several additional winters. This would increase the statistical power of the screening stage and reduce the need for a relaxed significance threshold, and would also enlarge the sample available for fitting the multivariate models, where the ratio of observations to estimated parameters is currently a limitation. Applying the same framework across several reanalysis products, as Lavers et al. (2012) did, would further test the robustness of the identified relationships to reanalysis uncertainty.

6. Conclusion

The study developed and compared a hierarchy of statistical methods, comprising correlation screening, phase-composite analysis, linear regression, GLM, and GAM, in order to identify the climate patterns that determine the frequency of winter AR events in the Western Himalayas and to evaluate their predictive capacity. Previously, more extensive studies had not dealt with this issue.

When we first examined the eighteen climate mode indices, we found that AO, PDO, PNA, EA-WR, and Sib-H had the strongest connections to winter AR frequency, with EA-WR being the most significant. Later, a phase-composite analysis confirmed these statistical links. In every case, the phase that led to higher IVT matched the direction of the mode's correlation with AR frequency (AO+ and EA-WR+; PDO− and PNA−). This means the associations show a real and consistent change in moisture transport, not just a random link. Both the AR count and the continuous atmospheric field back up these results, which makes us more confident in the physical basis of the predictors, not just their statistical correlation.

Linear regressions based on a single predictor showed that no one climate mode accounted for a large share of the variability in AR, RMSE values remaining very close within the range of 2.27 to 2.33 for all five modes. EA-WR was the most effective predictor on its own. When a multivariate GLM was employed with interaction terms (Sib-H × AO, EPNP × PNA, PNA × Niño4), there was a modest gain in out-of-sample predictive accuracy; although, its LOOCV RMSE was a bit higher than that of the single-predictor baseline due to few extremes, but the its predictive accuracy in the AR variability was much more accurate. This finding shows that adding more predictors and interaction terms to a linear model improve predictive ability for this dataset. The GAM, which allowed the EA-WR, EPNP × PNA, and WP × EPNP effects to take a nonlinear, spline-based form, greatly exceeded both the linear baseline and the GLM in all the evaluation criteria. The difference in performance between the GLM and GAM is important because it shows that the relationship between large-scale climate variability and winter AR frequency in the Western Himalayas is nonlinear. This nonlinearity, rather than simply adding more predictors, leads to much better predictions.

Putting the results together it becomes clear that the frequency of winter AR events in the Western Himalayas is the result of the combined and in part nonlinear influence of a number of climate patterns and is not controlled by any one single factor, unlike in places such as the British Isles where it was found that a single pattern (the Scandinavian Pattern) was enough to account for the variability in winter aridity events (Lavers et al., 2012). To our knowledge, this study is the first to directly compare linear and nonlinear multivariate statistical methods for predicting winter AR events in the Western Himalayas and the predictive power shown by the GAM framework, even though it is based on a record covering only 39 years, indicates real potential for using information from large-scale climate modes in the seasonal forecasting of AR-related precipitation and of variability in water resources in this sparsely observed, topographically complex and hydrologically important region.

References

Abid, M. A., Ashfaq, M., Kucharski, F., Evans, K. J., & Almazroui, M. (2020). Tropical Indian Ocean Mediates ENSO Influence Over Central Southwest Asia During the Wet Season. *Geophysical Research Letters*, *47*(18). https://doi.org/10.1029/2020GL089308

Athanasiadis, P. J., Wallace, J. M., & Wettstein, J. J. (2010). Patterns of Wintertime Jet Stream Variability and Their Relation to the Storm Tracks*. *Journal of the Atmospheric Sciences*, *67*(5), 1361–1381. https://doi.org/10.1175/2009JAS3270.1

Castellano, C. M., DeFlorio, M. J., Gibson, P. B., Delle Monache, L., Kalansky, J. F., Wang, J., Guirguis, K., Gershunov, A., Ralph, F. M., Subramanian, A. C., & Anderson, M. L. (2023). Development of a Statistical Subseasonal Forecast Tool to Predict California Atmospheric Rivers and Precipitation Based on MJO and QBO Activity. *Journal of Geophysical Research: Atmospheres*, *128*(6). https://doi.org/10.1029/2022JD037360

Chen, Z., Gan, B., Huang, F., Li, J., Wu, L., Fan, L., & Diao, Y. (2023). The influence of Pacific-North American teleconnection on the North Pacific SST anomalies in Wintertime under the global warming. *Climate Dynamics*, *60*(5–6), 1481–1494. https://doi.org/10.1007/s00382-022-06398-8

DeFlorio, M. J., Waliser, D. E., Guan, B., Lavers, D. A., Ralph, F. M., & Vitart, F. (2018). Global Assessment of Atmospheric River Prediction Skill. *Journal of Hydrometeorology*, *19*(2), 409–426. https://doi.org/10.1175/JHM-D-17-0135.1

Dong, W., Zhao, M., Tan, Z., & Ramaswamy, V. (2024). Atmospheric rivers over eastern US affected by Pacific/North America pattern. *Science Advances*, *10*(4). https://doi.org/10.1126/sciadv.adj3325

Gadgil, S., Vinayachandran, P. N., Francis, P. A., & Gadgil, S. (2004). Extremes of the Indian summer monsoon rainfall, ENSO and equatorial Indian Ocean oscillation. *Geophysical Research Letters*, *31*(12). https://doi.org/10.1029/2004GL019733

Gelaro, R., McCarty, W., Suárez, M. J., Todling, R., Molod, A., Takacs, L., Randles, C. A., Darmenov, A., Bosilovich, M. G., Reichle, R., Wargan, K., Coy, L., Cullather, R., Draper, C., Akella, S., Buchard, V., Conaty, A., da Silva, A. M., Gu, W., … Zhao, B. (2017). The Modern-Era Retrospective Analysis for Research and Applications, Version 2 (MERRA-2). *Journal of Climate*, *30*(14), 5419–5454. https://doi.org/10.1175/JCLI-D-16-0758.1

Gershunov, A., Shulgina, T., Ralph, F. M., Lavers, D. A., & Rutz, J. J. (2017). Assessing the climate-scale variability of atmospheric rivers affecting western North America. *Geophysical Research Letters*, *44*(15), 7900–7908. https://doi.org/10.1002/2017GL074175

Gong, D., Wang, S., & Zhu, J. (2001). East Asian Winter Monsoon and Arctic Oscillation. *Geophysical Research Letters*, *28*(10), 2073–2076. https://doi.org/10.1029/2000GL012311

Guan, B., & Waliser, D. E. (2015). Detection of atmospheric rivers: Evaluation and application of an algorithm for global studies. *Journal of Geophysical Research: Atmospheres*, *120*(24), 12514–12535. https://doi.org/10.1002/2015JD024257

Guan, B., Waliser, D. E., Molotch, N. P., Fetzer, E. J., & Neiman, P. J. (2012). Does the Madden–Julian Oscillation Influence Wintertime Atmospheric Rivers and Snowpack in the Sierra Nevada? *Monthly Weather Review*, *140*(2), 325–342. https://doi.org/10.1175/MWR-D-11-00087.1

Guirguis, K., Gershunov, A., Shulgina, T., Clemesha, R. E. S., & Ralph, F. M. (2019). Atmospheric rivers impacting Northern California and their modulation by a variable climate. *Climate Dynamics*, *52*(11), 6569–6583. https://doi.org/10.1007/s00382-018-4532-5

Hastie, T. J., & Tibshirani, R. J. (2017). *Generalized Additive Models*. Routledge. https://doi.org/10.1201/9780203753781

Lavers, D. A., Villarini, G., Allan, R. P., Wood, E. F., & Wade, A. J. (2012). The detection of atmospheric rivers in atmospheric reanalyses and their links to British winter floods and the large-scale climatic circulation. *Journal of Geophysical Research: Atmospheres*, *117*(D20). https://doi.org/10.1029/2012JD018027

Li, C., Mei, W., & Kamae, Y. (2022). Variability and predictability of cold-season North Atlantic atmospheric river occurrence frequency in a set of high-resolution atmospheric simulations. *Climate Dynamics*, *58*(9–10), 2485–2500. https://doi.org/10.1007/s00382-021-06017-y

Li, W., & Forest, C. E. (2014). Estimating the Sensitivity of the Atmospheric Teleconnection Patterns to SST Anomalies Using a Linear Statistical Method. *Journal of Climate*, *27*(24), 9065–9081. https://doi.org/10.1175/JCLI-D-14-00231.1

Linkin, M. E., & Nigam, S. (2008). The North Pacific Oscillation–West Pacific Teleconnection Pattern: Mature-Phase Structure and Winter Impacts. *Journal of Climate*, *21*(9), 1979–1997. https://doi.org/10.1175/2007JCLI2048.1

McCullagh, P., & Nelder, J. A. (2019). *Generalized Linear Models*. Routledge. https://doi.org/10.1201/9780203753736

McGregor, G. (2024). *Modes of Climate Variability* (pp. 169–206). https://doi.org/10.1007/978-3-031-69906-1_5

Mundhenk, B. D., Barnes, E. A., Maloney, E. D., & Baggett, C. F. (2018). Skillful empirical subseasonal prediction of landfalling atmospheric river activity using the Madden–Julian oscillation and quasi-biennial oscillation. *Npj Climate and Atmospheric Science*, *1*(1), 20177. https://doi.org/10.1038/s41612-017-0008-2

Nash, D., Carvalho, L. M. V., Jones, C., & Ding, Q. (2022). Winter and spring atmospheric rivers in High Mountain Asia: climatology, dynamics, and variability. *Climate Dynamics*, *58*(9–10), 2309–2331. https://doi.org/10.1007/s00382-021-06008-z

Nayak, M. A., Azam, M. F., & Lyngwa, R. V. (2021). *ERA5-based database of Atmospheric Rivers over Himalayas*. https://doi.org/10.5194/essd-2020-397

Panagiotopoulos, F., Shahgedanova, M., Hannachi, A., & Stephenson, D. B. (2005). Observed Trends and Teleconnections of the Siberian High: A Recently Declining Center of Action. *Journal of Climate*, *18*(9), 1411–1422. https://doi.org/10.1175/JCLI3352.1

Payne, A. E., Demory, M.-E., Leung, L. R., Ramos, A. M., Shields, C. A., Rutz, J. J., Siler, N., Villarini, G., Hall, A., & Ralph, F. M. (2020). Responses and impacts of atmospheric rivers to climate change. *Nature Reviews Earth & Environment*, *1*(3), 143–157. https://doi.org/10.1038/s43017-020-0030-5

Soulard, N., Lin, H., & Yu, B. (2019). The changing relationship between ENSO and its extratropical response patterns. *Scientific Reports*, *9*(1), 6507. https://doi.org/10.1038/s41598-019-42922-3

Toride, K., & Hakim, G. J. (2021). Influence of Low-Frequency PNA Variability on MJO Teleconnections to North American Atmospheric River Activity. *Geophysical Research Letters*, *48*(13). https://doi.org/10.1029/2021GL094078

Wallace, J. M., & Gutzler, D. S. (1981). Teleconnections in the Geopotential Height Field during the Northern Hemisphere Winter. *Monthly Weather Review*, *109*(4), 784–812. https://doi.org/10.1175/1520-0493(1981)109<0784:TITGHF>2.0.CO;2

Wood, S. N. (2017). *Generalized Additive Models*. Chapman and Hall/CRC. https://doi.org/10.1201/9781315370279

Xu, G., Wang, L., & Wang, S. (2023). Leading Modes of Wintertime North Pacific Atmospheric Rivers and Their Drivers. *Journal of Geophysical Research: Atmospheres*, *128*(5). https://doi.org/10.1029/2022JD037719

Yang, Z., DeFlorio, M. J., Sengupta, A., Wang, J., Castellano, C. M., Gershunov, A., Guirguis, K., Slinskey, E., Guan, B., Delle Monache, L., & Ralph, F. M. (2024). Seasonality and climate modes influence the temporal clustering of unique atmospheric rivers in the Western U.S. *Communications Earth & Environment*, *5*(1), 734. https://doi.org/10.1038/s43247-024-01890-x

Zhou, Y., & Kim, H.-M. (2018). Prediction of atmospheric rivers over the North Pacific and its connection to ENSO in the North American multi-model ensemble (NMME). *Climate Dynamics*, *51*(5–6), 1623–1637. https://doi.org/10.1007/s00382-017-3973-6

Zhu, Y., & Newell, R. E. (1998). A Proposed Algorithm for Moisture Fluxes from Atmospheric Rivers. *Monthly Weather Review*, *126*(3), 725–735. https://doi.org/10.1175/1520-0493(1998)126<0725:APAFMF>2.0.CO;2